International Journal of Earth Sciences (2022) 111:2225–2238
https://doi.org/10.1007/s00531-022-02241-x

ORIGINAL PAPER

Lithogenesis of a phosphatized tephra marker horizon in the Eocene Messel maar lake

Moritz Liesegang[1] · **Michael Wuttke**[2]

Received: 6 March 2022 / Accepted: 28 July 2022 / Published online: 13 August 2022

Abstract

The bituminous black pelite of the Messel UNESCO world heritage site is an exceptional palaeobiological archive from the Middle Eocene greenhouse climate. The pronounced homogeneity of the annually laminated pelite through a time interval of 640 kyr complicates the relative stratigraphic classification of fossil remains and is, thus, largely dependent on particular marker horizons within the uniform sedimentary column. We analyzed the most prominent marker horizon M using petrographic microscopy, X-ray powder diffraction, and electron probe microanalyses to identify and characterize its structure and phosphate-dominated mineralogy. Based on our analytical data, we suggest that this phosphatic marker horizon resulted from the exceptional combination of external tephra enclosed in bacteria and algae-rich layers, producing a coupled phosphorus and cation diffusion during diagenesis. Mantienneite ($KMg_2Al_2Ti(PO_4)_4(OH)_3 \bullet 15H_2O$) is documented for the first time in the Messel fossil deposit. The diagenetic succession of messelite, montgomeryite, and mantienneite precipitation reflects the internal heterogeneities in primary mineral composition of an ash layer. Kerogen maturation and hydrocarbon migration produced acidic, reducing pore fluids with high P concentration, which enhanced the mobility of Al and Ti. The mantienneite-forming reaction marks the change from a regime of reducing to oxidizing conditions. With the deposition and diagenesis of the marker horizon M, a singular event is preserved in a sedimentary sequence otherwise regarded as largely uniform over a time span of about 640 kyr.

Keywords Messel · Eocene · Maar lake · Mantienneite · Tephra · Phosphatization

Introduction

The Lower to Middle Eocene bituminous, finely laminated black pelite ('oil shale'; Lenz et al. 2015) of the Messel UNESCO world heritage site near Darmstadt, Germany (Fig. 1), is famous for its unique, exceptionally well-preserved fossils. Since the 1970s, scientific excavations took place in the former open-cast mine, with the aim, among others, to reconstruct changes in the fossil composition in space and time as well as identify inherent changes in paleoclimate and biodiversity (e.g., Lenz et al. 2011, 2015; Micklich 2002, 2012; Tütken 2014; Richter et al. 2017; Lenz and Wilde 2018). The sediments were deposited in a nearly isolated Eocene maar lake (Schulz et al. 2002; Felder and Harms 2004) with occasional inflows during water high stands in the surroundings (Micklich 2002, 2012; Richter et al. 2013). In his comprehensive work on the Messel sediments, Goth (1990) described a 140 m thick sequence of 'oil shale' (Middle Messel Formation, Weber and Hofmann 1982). Another 60 m thick black pelite on the top was mined during industrial use in the nineteenth and twentieth century. During the lithogenesis of the Messel black pelite, facies conditions and sedimentation rate remained stable (Goth 1990; Lenz et al. 2011). Based on a constant sedimentation rate of 0.14 mm/year, a finely laminated, highly bituminous pelite formed during a long-term stable meromictic phase, which might have lasted about 640 kyr (Lenz et al. 2011, 2015; Lenz and Wilde 2018).

✉ Moritz Liesegang
m.liesegang@fu-berlin.de

Michael Wuttke
michael.wuttke@senckenberg.de

[1] Institut für Geologische Wissenschaften, AB Mineralogie-Petrologie, Freie Universität Berlin, Malteserstr. 74-100, 12249 Berlin, Germany

[2] Senckenberg Forschungsinstitut und Naturmuseum, Section Palaeoclimate and Environmental Research, Division of Messel Research and Mammalogy, Senckenberganlage 25, 60325 Frankfurt am Main, Germany

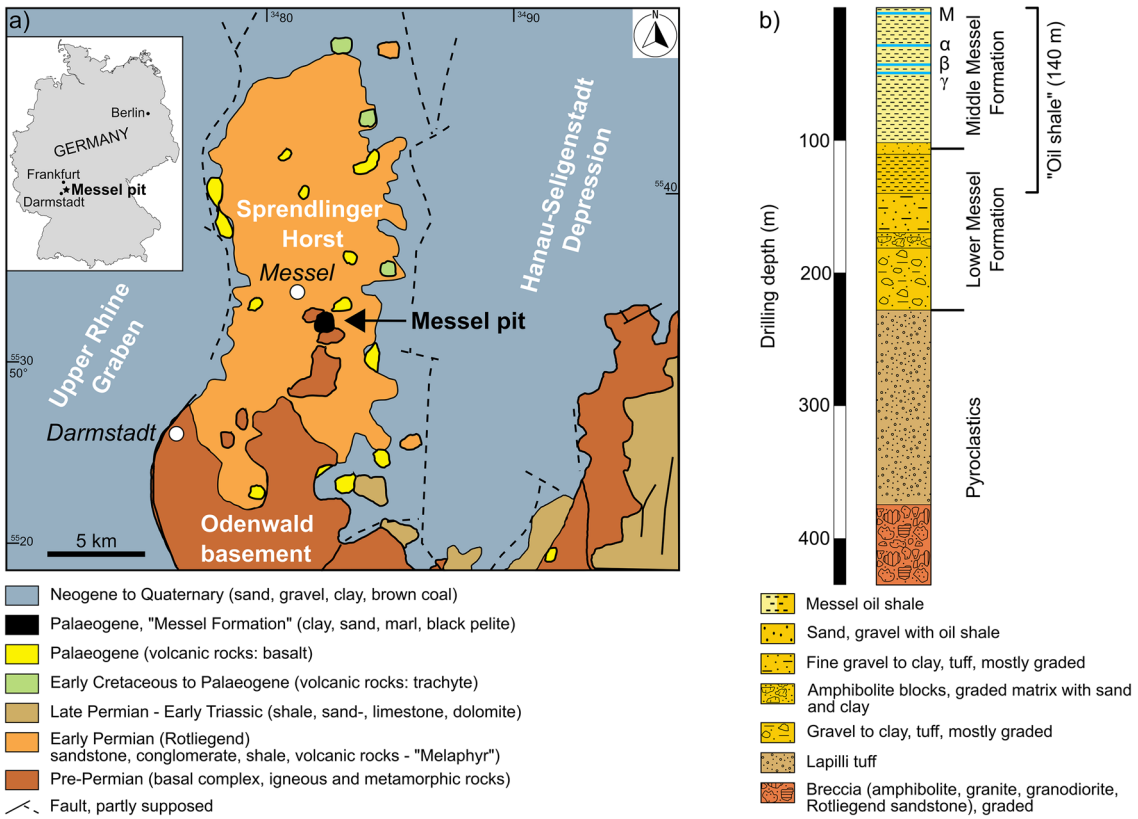

Fig. 1 **a** Geological map showing the location of the Messel pit in relation to other Palaeogene sites in the area (modified after Harms et al. 1999; Lenz et al. 2011), **b** Profile of the Messel 2001 core including the oil shale (black pelite) with positions of the marker horizons M (3.91 m), α (27.36 m), β (42.4 m), and γ (44.4 m) (modified after Franzen et al. 1982; Felder and Harms 2004; Lenz et al. 2011)

The macroscopically uniform appearance of the black pelite naturally complicates the stratigraphic classification of fossils during excavations. Several marker horizons were discovered in the Middle Messel Formation (MMF) that facilitate the relative stratigraphic classification (Fig. 1). So far, the stratigraphically oldest marker horizons, α, β, and γ (Franzen et al. 1982), have been described macroscopically but not analyzed in detail. It has been suspected that the marker horizons α and β are tephra (Weber 1988). Another marker horizon, the so-called "double messelite horizon" (Muthmann 1890), was recognized as an additional marker horizon for excavations younger than α (Schaal et al. 1987). Messelite crystal growth in this horizon almost completely erased the primary sedimentary structures (Goth 1990).

This study focusses on the youngest marker horizon, the "Marker Horizon M" (MH M; Schaal et al. 1987) that consists of an up to 30 mm thick tripartite layer of phosphate minerals, with bands of messelite crystals enclosing a montgomeryite-rich band (Schaal 1992; Schaal et al. 1987; Goth 1990; Felder and Harms 2004; Felder 2007; Fleck and Kolitsch 2003). The thickness of the material studied here varies from ~ 15 to 20 mm within a few centimeters distance. However, the phosphatic horizon is usually considered to show a fairly uniform thickness and mineralogy across the entire former maar lake (Felder and Harms 2004) and is commonly used as a reference horizon for the relative stratigraphic positions of fossils (e.g., Micklich 2012; Tütken 2014; Richter et al. 2017).

Various hypotheses exist on the formation of MH M. Previous studies agree that the marker horizon precipitated directly at the sediment–lake interface with an external or internal phosphorus source. After Schaal et al. (1987) and Schaal (1992), the formation and arrangement of the crystal aggregates show that the phosphate mineral layer formed directly at the lake bottom. The source material is suspected to be a phosphate sludge representing a single event that marks a special hydrochemical and time-limited process within the normal sedimentation sequence. A phosphate-rich surface inflow from the hinterland or by phosphate-saturated groundwater inflow could have transported the source material. Goth (1990) rejected the phosphate sludge hypothesis of Schaal et al. (1987) and postulated a precipitation at the sediment–water interface that resulted from an upward P-rich fluid influx from the sediment into the lake water at

anaerobic conditions. The chemical processes required for this process have yet to be explained. Felder (2007) advocates a microbial mat hypothesis. In this scenario, MH M formed when all the water of the normally meromictic Lake Messel became oxygen rich for a short time so that an aerobic microbial mat grew on the sediment surface. Only little phosphorus could dissolve in the water column near the sediment–water interface. As a result, a strong concentration gradient existed between the phosphate-rich pore water and the phosphate-poorer lake water, so that phosphate in the pore water migrated toward the microbial mat-covered sediment surface. After the onset of anoxic conditions, phosphate accumulated in the microbial mat was released, which subsequently led to montgomeryite and messelite precipitation from the lake bottom water (Felder 2007).

In this study, we use X-ray powder diffraction and electron microprobe analysis to characterize the structure and mineralogy of the MH M. We use these results to clarify the precursor composition and depositional mode of MH M, and identify the diagenetic mineral precipitation sequence. To the best of our knowledge, this study provides the first clear evidence for a singular tephra deposition event in the fossil-rich Messel sedimentary sequence otherwise regarded as largely uniform through a time interval of about 640 kyr. Our results and model may also provide an important contribution to the study of the response of ecosystems in volcanically disturbed habitats and diagenetic phosphatization processes coupled with hydrocarbon mobilization in organic-matter-rich environments.

Geological setting

The Messel pit is located on the Sprendlinger Horst, the northern extension of the Odenwald Mountains basement, which is flanking the Upper Rhine Graben to the northeast in Southwest Germany (Fig. 1a). The Sprendlinger Horst consists of a Paleozoic metamorphic and magmatic basement with a cover of Rotliegend (Lower Permian) sediments and Permian basaltic lava flows ("Melaphyr") (Marell 1989). Several small, nowadays isolated basins filled by lacustrine sediments of Paleogene age are known from the area, some of which have been studied from drill cores and mining. Most of them represent the filling of maar-type volcanic structures (e.g., Jacoby et al. 2000; Felder and Harms 2004; Moshayedi et al. 2018, 2020). This includes the Eocene maar lake of Messel, which is well known for the exceptional preservation of fossils and was a goal of numerous paleoenvironmental studies (e.g., Lenz et al. 2007, 2011; Richter et al. 2017).

Associated with the Upper Rhine Graben formation, intraplate magmatism and volcanism were initiated, apparently influenced by the Alpine collision-related stress regime (Sissingh 2003). Several small Tertiary volcanoes are located along the northern margin of the URG, i.e., in the Taunus Mountains of the Hunsrück–Taunus Mountain Range and on the eastern shoulder of the northern URG, i.e., the Sprendlinger Horst (e.g., Berger et al. 2005a,b; Reischmann et al. 2011; Lutz et al. 2013). More than 30 locations of deeply eroded volcanoes (< 200 m) and proven maars on the Sprendlinger Horst document the Paleogene off-rift volcanism (Maccaferri et al. 2014; Büchel and Schaal 2018). This Early Paleogene volcanism shows its main phase of activity on the Sprendlinger Horst as low-SiO_2 volcanism between ca. 50 and 45 Ma (Mertz and Renne 2005; Lenz et al. 2015). The former maar filling of Messel is the best known and studied occurrence of Paleogene sediments on the Sprendlinger Horst.

The Messel phreatomagmatic eruptions are attributed to the reactivation of a Variscan "Messel Fault Zone" during initial opening of the Upper Rhine Graben (Jacoby et al. 2000; Mezger et al. 2013). Prior to the formation of the Messel Maar, there existed a massive sequence (of unknown thickness) of country rock consisting of breccia, conglomerates, massive basaltic lava flows from the Saar Nahe Basin (Melaphyr) in the WSW, and sandstone, all from the Lower Rotliegend (Permian; Marell 1989). Today, the sequence is preserved as relicts with a maximum thickness of 66 m near the pit's eastern edge (Marell 1989; Felder and Harms 2004). Below this sedimentary cover, the Sprendlinger Horst bedrock around Messel consists of granodiorites, diorites, and amphibolites as shown by analysis of the diatreme breccia section of the scientific well Messel 2001 (Felder and Harms 2004; Mezger et al. 2013).

The phreatomagmatic eruptions ended with 130 m thick lapilli to ash tuffs, with lapilli tuffs clearly predominating. Juvenile parts are mainly basaltic ashes and spherical lapilli of 1–20 mm diameter. Parts of the accretionary lapilli have a nucleus of granodiorites, amphibolites, or titaniferous magnetite (Felder and Harms 2004; Nitzsche et al. 2006). These rocks formed the Messel Maar crater wall to varying degrees, with the youngest layers of the crater wall likely to have consisted preferentially of basaltic accretionary lapilli tuffs and ashes. All the Eocene country rock within the crater wall contributed to the Messel black pelite in form of runoffs of weathering debris and solutions.

Lithology

The classical "Messel oil shale" of the Middle Messel Formation (MMF) is characterized by a more than 90 m thick continuous succession of finely laminated bituminous pelite (Weber and Hofmann 1982; Felder and Harms 2004; Lenz et al. 2011) with several marker horizons (Fig. 1b). This pelite represents a long-term stable meromictic phase in Lake Messel without major sedimentological fluctuations over a period of about 640 kyr (Goth 1990; Lenz et al. 2011).

The alternation of fine dark and light laminae reflects an annual stratification caused by blooms of the coccal green alga *Tetraedron minimum* (light laminae), or, in the upper part of the MMF, by the green alga *Botryococcus* sp. interrupting a continuous background sedimentation (dark, bituminous clays) (Goth 1990; Lenz et al. 2007).

The black pelite is mainly composed of smectite with minor kaolinite, illite, and zeolites (cf. Weber and Zimmerle 1985; Kubanek et al. 1988). Traces of potassium feldspar show a high barium content and those of biotite a marked chromium content. Prismatic chlorapatite is a typical accessory mineral in heavily altered rock fragments of presumably basic volcanic origin. The shale matrix contains abundant mixed Fe–Ti oxides and minute Cr-spinel. Major and trace element compositions of the Messel black pelite deviate significantly from the worldwide clay and shale average. It displays low Na_2O and K_2O, high TiO_2 and Fe_2O_3, as well as high V, Sr, Zr, and Nb. Most analyses fall into the basanite–nephelinite field providing strong evidence for the basic volcanic ancestry of the Messel black pelite (Kubanek et al. 1988). After deposition, the primary mafic minerals such as olivine, pyroxene, and/or hornblende quickly altered to clay minerals (Kubanek et al. 1988). The phosphate content of the sediment averages between 0.91 and 3.20% P_2O_5, according to analyses from the mining area (Matthess 1966).

After the biogenic and abiogenic sedimentation, several authigenic minerals formed during early diagenesis (e.g., Goth 1990; Felder 2001), of which the phosphates of MH M are of interest here. A locally high phosphate content in the pore water of the Messel sediments is evidenced by two dm thick horizons with minor randomly distributed messelite crystal aggregates (double messelite horizon; Muthmann 1890; Schaal et al. 1987; Goth 1990), phosphatized algae (Richter et al. 2013), and a microbially mediated phosphatization of fish and crocodile coprolites (Schmitz 1991; Liebig et al. 1996).

Materials and analytical methods

The material was sampled on the lowest level of the Messel pit (center of the basin; see Fig. 1 in Schaal et al. 1987 for the distribution of MH M), 8 km north of Darmstadt (Germany) and is deposited in the Mineralogical Section of the Senckenberg Research Institute in Frankfurt M under the collection number SMF 12639a. Another piece of the sample is deposited in the Mineralogical Collections of the Museum of Mineralogy and Geology in Dresden (Collection No SMF 12639b).

X-ray powder diffraction data were recorded on a PANalytical Empyrean diffractometer using CuKα radiation (λ = 1.54060 Å) at 40 kV and a tube current of 40 mA. Samples were prepared with a diamond file and scanned on a rotating stage at 2.5°2θ/min (step size 0.013°2θ) from 7 to 60°2θ. Polished, carbon-coated thin sections were prepared for electron microprobe analysis (EMPA) and backscattered electron (BSE) imaging. A JEOL JXA 8200 Superprobe, operated at an acceleration voltage of 15 kV, 20 nA beam current, and 5 µm beam diameter was used to determine the chemical composition of individual minerals using the wavelength-dispersive (WDX) detectors. The acquisition time for Na analysis was 5 s on peak and 5 s on background. The peak and background of other elements were measured for 10 s each. The spatial distribution of Si, Ti, Al, Fe, Mg, Ca, Na, K, P, and S was mapped at a probe current of 30 nA and 80 ms counting time per 15 µm pixel size (beam diameter of 1 µm).

Results

Petrographic microscopy (Fig. 2) and powder X-ray diffraction (Fig. 3) show that the marker horizon M consists of phosphates and trace silicates forming three texturally and mineralogically distinct bands separated by a black pelite layer: (i) a ~ 6 mm thick lower band of radial, flattened aggregates of columnar messelite crystals, (ii) a ~ 9 mm thick central band dominated by montgomeryite globules embedded in a messelite groundmass and extensively replaced by the Ti–K phosphate mantienneite, and (iii) a ~ 5 mm thick upper messelite band consisting of parabolic bundles of upright columnar crystals. In contrast to the upper messelite band showing an upward crystal growth direction, messelite at the interface of the central band with the lower messelite band consists of an about 80 µm thick veinlet of downward pointing parabolic bundles, followed by radial, flattened aggregates. Importantly, only the lower and upper messelite bands contain laminated black pelite fragments. These are commonly fractured and bent by messelite crystal growth (Fig. 2b–c). A late generation of messelite fills vertical veins that transition into narrow ridges on the marker horizon surface.

While the lower and upper messelite bands have a comparably uniform mineralogical composition, the central band shows complex intergrowth and replacement relationships between phosphates and relict primary minerals (Fig. 4). The chemical composition of phosphates obtained with electron microprobe WDX spot analysis is collated in Table 1. The most abundant silicates in the central band are micrometer-sized silica spheres and sphere agglomerates. Silica spheres occur in messelite and as an infilling of crystal and glass shard-shaped pore space in mantienneite (Fig. 4b, d). EMP–WDX spot analysis of the silica spheres yields a composition (in wt%): SiO_2 ~ 96, Al_2O_3 0.31, FeO_{total} 0.08, and K_2O 0.06, on average. Their spherical micromorphology

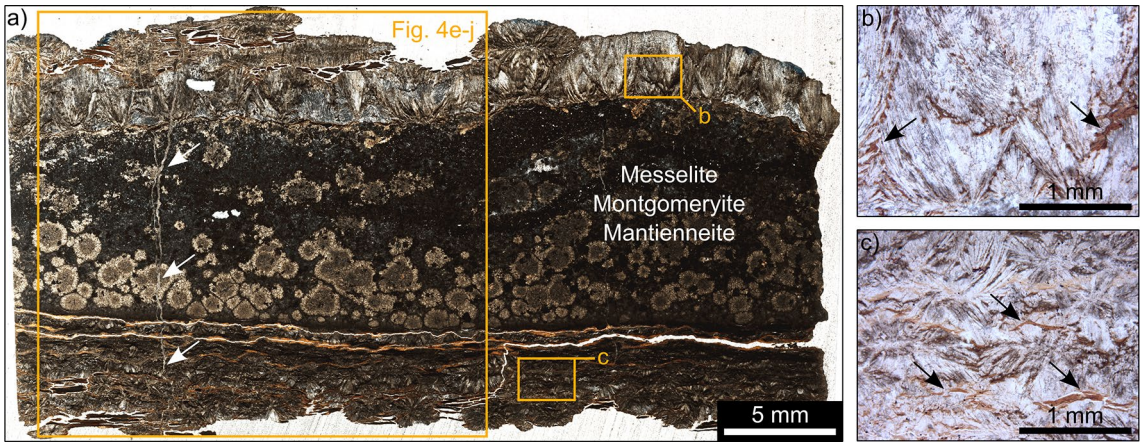

Fig. 2 Thin section micrographs of the marker horizon **a** and its lower and upper messelite bands **b**–**c**, a The top and bottom messelite bands comprise of messelite intercalated with black pelite fragments and enclose a central band with a messelite groundmass, zoned montgomeryite globules, and mantienneite. Vertical messelite veins (left side, white arrows) crosscut the entire marker horizon. The large highlighted area was selected for detailed WDX element distribution mapping (Fig. 4e-j), **b**–**c** Black pelite (dark brown color; black arrows) is bend and fractured by early parabolic (**b**) and radial (**c**) messelite crystal growth in the upper and lower band, respectively, indicating black pelite deformation and fracture after consolidation

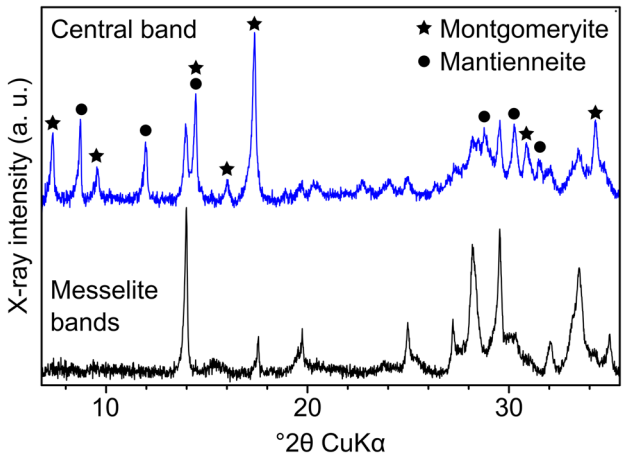

Fig. 3 Diffractograms of the lower and upper messelite bands (bottom) and the central montgomeryite-rich band (top) of the Messel marker horizon M. The messelite bands are primarily free of mineral impurities other than minor black pelite. The central band contains messelite and abundant montgomeryite (stars) and mantienneite (circles). Diffractograms are shifted for clarity

and chemical composition are consistent with opal-A (e.g., Liesegang and Milke 2014).

In the central band, messelite (idealized formula $Ca_2(Fe^{2+}, Mn^{2+})(PO_4)_2 \bullet 2H_2O$) forms the groundmass and occurs as corroded blocky crystals with well-developed cleavage and less commonly as radially fibrous globules (Fig. 4a, b). The chemical composition of messelite in the entire marker horizon differs insignificantly, which includes the late vertical vein. Montgomeryite forms ~ 200–2000 µm large globules consisting of radially fibrous crystals (idealized formula $Ca_4MgAl_4(PO_4)_6(OH)_4 \bullet 12H_2O$). Occasionally, montgomeryite replaces messelite in the form of slender prisms (Fig. 4b). The bottom messelite band contains very few montgomeryite globules < 50 µm (Fig. 4i). Among the phosphates in the marker horizon, only montgomeryite contains trace quantities of relict apatite, Fe oxide/hydroxide, ilmenite, pyrite, alkali feldspar (~ 50% albite), TiO_2, and titanite, generally with crystal sizes < 30 µm (Fig. 4a, c). Most of the enclosed ilmenite is extensively corroded to TiO_2 and Fe oxide/hydroxide. Trace mineral impurities produce a core-rim zoning (dark core, light rim) of the globules in transmitted light.

Element distribution mapping and BSE imaging show that mantienneite (idealized formula $KMg_2Al_2Ti(PO_4)_4(OH)_3 \bullet 15H_2O$) occurs dominantly in the upper half of the central band (Fig. 4). Mantienneite develops radially columnar to fibrous spherules and rarely single columnar crystals, replaces montgomeryite globules and the messelite groundmass, and forms bands with abundant silica-filled pore space. This pore space is up to ~ 100 µm large, randomly oriented, and resembles stubby prismatic crystals and glass shards with platy morphology (Fig. 4d).

Discussion

We used petrographic microscopy, powder X-ray diffraction, and electron beam microanalysis to identify and characterize the structure and mineralogy of the singular marker horizon M in the Lower to Middle Eocene bituminous black pelite of the maar lake Messel. The marker horizon represents a short exceptional sedimentation episode with a

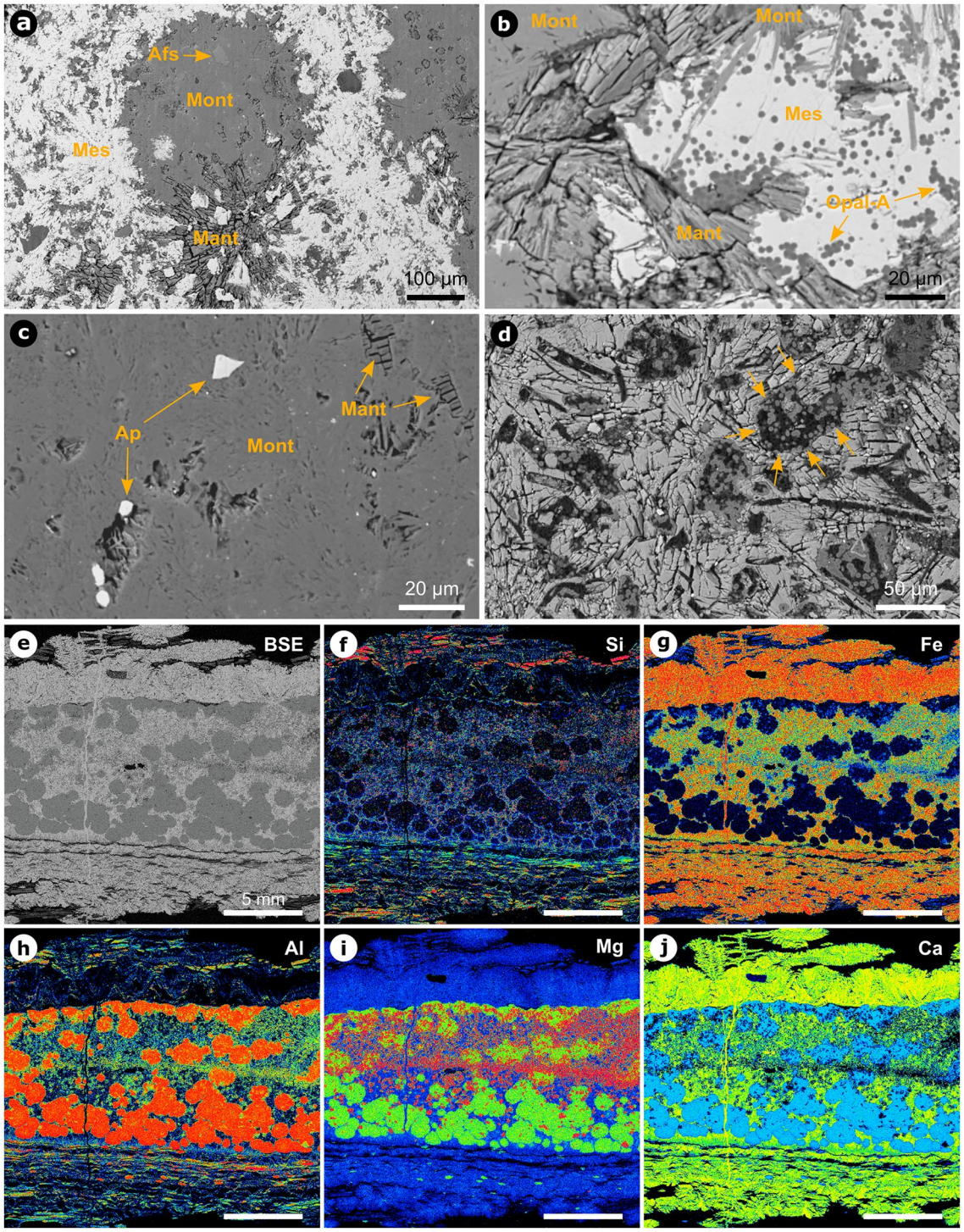

Fig. 4 BSE images **a**–**d** of the mineral assemblage in the central band and quantitative WDX maps **e**–**j** across the marker horizon M, **a** Montgomeryite (Mont) globules in a messelite (Mes) matrix replaced by mantienneite (Mant). Only montgomeryite contains relict primary minerals, e.g., alkali feldspar (Afs), **b** Slender montgomeryite prisms and fibrous to columnar mantienneite replace messelite with abundant opal-A spheres, **c** Columnar mantienneite replaces montgomeryite with relict apatite (Ap), **d** Mantienneite enclosing partially silica sphere-filled pore space resembling stubby euhedral crystals (arrows) and glass shards, **e**–**j** WDX element distribution maps for Si, Fe, Al, Mg, and Ca of the marker horizon M. Silicon is enriched in black pelite layers and opal-A microspheres predominantly in messelite of the central band. Mantienneite has the highest Mg (**i**) and lowest Ca (**j**) concentration of the analyzed phosphates. Warmer colors represent higher concentrations

Table 1 Chemical composition (given in wt%) of phosphates by electron microprobe analysis. DL denotes detection limit. H_2O by difference

	Messelite	Messelite vein	Montgomeryite	Mantienneite
P_2O_5	39.09	38.73	35.95	32.18
TiO_2	< DL	< DL	0.25	8.95
Al_2O_3	0.06	0.16	16.34	10.81
FeO_{total}	14.09	13.90	1.19	3.03
MnO	2.65	3.40	0.13	0.22
MgO	1.43	1.19	3.37	7.69
CaO	30.99	31.01	18.72	0.44
Na_2O	< DL	< DL	< DL	0.18
K_2O	< DL	< DL	< DL	3.85
H_2O	11.69	11.62	24.05	32.66
Na	–	–	–	0.05
K	–	–	–	0.72
Fe^{2+}	0.71	0.71	–	–
Mn	0.14	0.17	0.02	0.03
Mg	0.13	0.11	0.99	1.68
Ca	2.01	2.02	3.95	0.07
Al	–	0.01	3.80	1.87
Fe^{3+}	–	–	0.18	0.33 *
Ti	–	–	–	0.99
P	2.00	2.00	6.00	4.00

Number of ions based on P = 2 (messelite), 6 (montgomeryite), and 4 (mantiennéite)

*According to Fransolet et al. (1984), Fe in mantienneite is Fe^{3+}

supraregional origin, which cannot be explained by run-off debris from the crater wall or from an external inflow by chemical and textural interpretation of the sediment. The phosphate mineral assemblage of messelite, montgomeryite, and mantienneite indicates a significant change of the sediment composition characterized by an enrichment of, e.g., P and Ti, that is exceptional during a Lake Messel depositional history of about 640 kyr (Lenz et al. 2011, 2015; Lenz and Wilde 2018). The vital elements to reconstruct the marker horizon formation are the precursor composition, phosphorus sources and transport, and fluid–mineral interaction processes that control the mineralogy.

Marker horizon precursor sediment

The formation of abundant montgomeryite and mantienneite within the marker horizon M implies a bifurcation of the depositional process and sediment precursor composition. The rather uniform thickness of the marker horizon across the entire Lake Messel and compositional singularity argues against sedimentary input from the crater wall. Trace minerals such as alkali feldspar, apatite, and mixed Fe–Ti oxides occur throughout the black pelite of the Middle Messel Formation (Weber and Zimmerle 1985; Kubanek et al. 1988) and the ~ 9 mm thick central band of the marker horizon. However, only the marker horizon contains montgomeryite and mantienneite. This indicates a significant change of the sediment composition not found elsewhere within 640 kyr of Lake Messel sedimentation (Lenz et al. 2011, 2015; Lenz and Wilde 2018). Apparently, the sediment that preceded the marker horizon did not derive from the weathered crater rim, but entered the lake via an alternative pathway, for example, a tephra cloud, as suspected previously for the older marker horizons α and β (Weber 1988). Mantienneite enrichment in the upper half of the central band could reflect a change in tephra composition, with an upward increasing Ti concentration. A potential cause for increasing grain sizes and changing compositions toward the top of the central band could be a two-phase eruption with a stronger second eruption that more violently vented tephra in a larger eruption cloud. Another possibility is crystal fractionation in a magma chamber. In this scenario, an early tephra layer formed the lower part of the central band, while Ti-rich minerals with high density (e.g., ilmenite, Ti-rich pyroxenes, etc.) were assimilated as xenocrysts during replenishment of a magma chamber and transported during protracted explosive volcanism. Thus, a second tephra cloud with a higher proportion of these minerals may have formed during an immediately following eruption. Together with glass shards, Lake Messel may then have accumulated Ti-rich minerals in a distinct horizon within the tephra band as a source for later mantienneite formation (Fig. 3d).

The original petrographic composition of MH M can only be incompletely reconstructed due to the strong alteration and phosphatic replacement of the primary minerals. Only the stubby shape of the pore spaces in mantienneite-rich domains, resembling euhedral crystals of pyroxene and feldspar, and the ions provided for the formation of the various phosphates, such as Al (relicts of feldspar and/or clay-sized Al-rich components), Mg, K (from alkali feldspar, biotite), and Ti (e.g., from pyroxene, amphibole, biotite, ilmenite), indicate an originally volcanogenic composition of the source sediment.

The micrometer-sized cavities left by dissolved ash particles and minerals in MH M suggest that crystals and shards originate from the distal parts of a faraway wind-driven ash cloud that partly settled over Lake Messel. Therefore, the nearby Eocene eruption centers on the Sprendlinger Horst, in the Taunus Mountains, or within the Upper Rhine Graben Rift Zone, the latter today buried under kilometers of younger Tertiary and Pleistocene sediments (Lutz et al. 2013), are less probable as a cause. In terms of grain size, distant ashes from the post-breakup North Atlantic Igneous Province (NAIP) or the pre-rift Massif Central, which were active in the time of Messel (Michon and Merle 2001; Meyer et al. 2007; Wilkinson et al. 2017) are potentially to

be considered (e.g., NAIP generated bentonites in Austria; Huber et al. 2003), but this is speculative, due to the intense diagenetic overprint of the precursor material.

Sources of phosphate

Various autochthonous and allochthonous sources contributed to the organic matter and associated phosphorus content of the Messel black pelite over time (Bauersachs et al. 2014). A considerable amount of phosphate input into Lake Messel results from internal organic matter, solutions from the paratropical soils by run off and groundwater, subaquatic alteration of pyroclastic particles, and weathered basanite-nephelinite crater rim debris (Kubanek et al. 1988). According to Porder and Ramachandran (2013) basanitic–nephelinitic basalts have median P concentrations from 3000 to 4000 µg/g. To a much lesser extent, crater wall material such as granodiorite (median 698 ppm), diorite (median 1004 ppm) and amphibolite (median 655 ppm) may have contributed to the phosphate content of the Messel black pelite (Mezger et al. 2013). The crater wall lithologies could partly provide P for phosphate precipitation and other elements of the marker horizon. However, the absence of a horizon similar to MH M suggests that the P content of the basanitic–nephelinitic precursor of the Messel oil shale was not enough to achieve the complete transformation of the exceptional marker horizon sediment into phosphate minerals. For this, an additional P supply was necessary.

This supply is likely related to the abundant sedimentary organic matter in the Middle Messel Formation. The high molar C_{org}/N_{tot} ratios of the Middle Messel Formation black pelite reflects a predominantly terrestrial origin of the preserved sedimentary organic matter. This includes plant litter from a dense paratropical rainforest near the maar lake. Comparatively heavy $\delta^{15}N_{tot}$ as well as high C_{org}/N_{tot} ratios and HI values of the of the sedimentary organic matter suggests a high number of lipid-rich constituents of vascular plants of the total organic matter (Bauersachs et al. 2014).

Autochthonous sources, for example, bacteria (stored as polyphosphates in granules, e.g., Cosmidis et al. 2014) and algae from the epilimnion of Lake Messel contributed in variable proportions to the organic matter content over time. Stable carbon isotope excursions to heavier $\delta^{13}C_{org}$ values indicate periods of increased algal productivity by different (pico-)phytoplankton species (e.g., cyanobacteria, Chrysophyta indet., the dinoflagellate *Messelodinium thielepfeifferae*, the coccal green algae *Tetraedron minimum*, *Botryococcus sp*. as well as *Coelastrum sp*.) and increased input of autochthonous organic matter to the lake sediments (Goth 1990; Lenz et al. 2011; Richter et al. 2013; Bauersachs et al. 2014). The overall depletion of $\delta^{13}C_{org}$ values together with an increase in $\delta^{15}N_{tot}$ values throughout the black pelite evidence microbial reworking of the sedimentary organic matter by methanogens, methanotrophs and denitrifiers (Bauersachs et al. 2014). Later, anaerobic digestion liberated organically bound phosphorus as orthophosphate into solution that may bind with cations including Mg, Ca, Al, Fe, and Ti to form the phosphate minerals that dominate the marker horizon M.

The exceptional phosphate accumulation associated with MH M is potentially linked to the input of the volcanic ash precursor into the water column. It has been shown that volcanic ash dissolving in lake- or seawater modifies the nutrient budget of the surface lake and ocean and stimulates the growth of phytoplankton, for example, in iron-limited lake/oceanic areas (e.g., Mattews-Bird et al. 2017; Duggen et al. 2007; Browning et al. 2015). The amount of bioavailable elements is directly proportional to the volcanic ash thickness (Duggen et al. 2007). Since ocean production and export of organic carbon transfers CO_2 from the atmosphere to the ocean interior, volcanic ash fertilization may play a vital role for the ocean–atmosphere gas interchange and ultimately the development of the global climate (Hamme et al. 2010; Hamilton et al. 2022). In oligotrophic lakes, volcanic ash input can result in 1.5- to eightfold increases in total suspended solids, light extinction, phosphorus concentrations, and phytoplankton biomass relative to pre-eruption conditions (Modenutti et al. 2013). Potentially, a transient micronutrient enrichment supplied by a volcanic ash resulted in intense bacteria and algae blooms in Lake Messel as well. Such blooms significantly enhance the diffusive fluxes of soluble reactive phosphate and iron from sediment pore water to the overlying water (Chen et al. 2018; Wang et al. 2022). While an increased pH value of the water column and upper sediment layer promotes the desorption of phosphate from mineral surfaces (Gao et al. 2014), anoxic conditions at the sediment–water interface cause the reductive dissolution of iron oxide minerals and the coupled release of iron and surface-bound P into pore water (Smith et al. 2011; Cosmidis et al. 2014).

The decomposition of algae during or after an algae bloom results in the release of P from degraded algal cells and re-release to the sediment and overlying water (Wang et al. 2022). Settling tephra particles in Lake Messel could also have adsorbed P from the water column and contribute significantly to the synsedimentary, exceptional P accumulation in the sediment within and adjacent to the later marker horizon. Early diagenesis mobilizes these accumulations and phosphorus diffuses and reacts with the volcanic ash. In this context, high-resolution palynological study (e.g., Moshayedi et al. 2020) of the sediment near the marker horizon M may contribute to our understanding of the response of ecosystems in a volcanically disturbed habitat, e.g., harmful bacteria or algae blooms in a lacustrine environment or the abrupt scarceness of Messel pit fishes, plants, and arthropod

remains after a volcanic eruption (e.g., Micklich, 2012; Lu et al. 2021).

Conclusively, the formation of the marker horizon requires a relative phosphorus enrichment to the typical black pelite sediment. Indicators for an exceptionally thick organic layer, such as a microbial mat grown on the sediment surface (Felder 2007), and bacteriomorphic phosphatic compartments (Schmitz 1991; Liebig et al. 1996) were not observed. The occurrence of black pelite in the messelite bands shows that it is unlikely that event sedimentation of weathered crater rim material directly provided the amount of phosphorus required for the formation of the marker horizon. Our results indicate that, contrary to earlier studies that favored a direct precipitation of the marker horizon at the sediment–lake interface (Schaal et al. 1987; Goth 1990; Felder 2007), it is more likely that phosphorus enrichment resulted from alteration of P-rich precursor sediment, e.g., phosphatized *Coelastrum*-algae layers (Richter et al. 2013) and P adsorbed to mineral surfaces, and subsequent pore water diffusion toward and within the marker horizon during diagenesis. Later phosphate mobilization from sediment below the marker horizon resulted in the formation of vertical messelite veins that crosscut the entire marker horizon.

Element transport and phosphate precipitation in the marker horizon

The diverse mineralogy of MH M indicates that the pore fluid composition changed continuously during diagenesis. The phosphate precipitation sequence records these changes that are likely related to, e.g., the specific surface area of primary minerals, primary mineral dissolution rates and sequence, and kerogen maturation (Curtis 1983; Weibel and Friis 2004; Wilson 2004; Sindern et al. 2019). Among the detrital minerals, those with a large specific surface area are most likely to be preserved as negative crystal shape, e.g., associated with mantienneite (Fig. 4d). Since the marker horizon mineralogy lacks indicators for vertical diffusion gradients, most mineral reactions can be considered to result from element re-distribution within the marker horizon. The low mobility of Al and Ti indicates that the marker horizon itself is the source and sink of these elements.

During diagenesis of the marker horizon, the pore fluid will repeatedly be out of equilibrium with primary and authigenic minerals. Thus, it is unavoidable that fluid-mediated, coupled mineral dissolution and precipitation processes will take place (Ruiz-Agudo et al. 2014). It should be noted that only trace amounts of minute non-phosphate minerals are preserved in the marker horizon. Thus, their scarcity lowers their value as geochemical indicators. Among the trace minerals, silica spheres in messelite are by far most abundant. They document the important role of silicate dissolution during phosphatization of the marker horizon.

Diagenetic processes alter the mineral components of the marker horizon as well as the organic material. Kerogen maturation and hydrocarbon mobilization is an omnipresent process in the Messel oil shale and can play an important role for pore fluid composition, mineral dissolution/precipitation, and element mobility (Curtis 1983; Waldmann and Gaupp 2016; Sindern et al. 2019). High molecular weight organic matter readily loses carbon dioxide, which is soluble and dissociates (Curtis 1983). This process not only produces acidified, reducing pore fluids but also releases large quantities of organically and mineral surface-bound phosphate. Further kerogen maturation is a constant source of these acidic, reducing fluids until the reducing agent (organic material) is exhausted (Weibel and Friis 2004).

Messelite bands

Messelite has been known from its type locality, the Messel pit, since 1890 (Muthmann 1890). Other sedimentary occurrences are the equally old deposits of the Prinz von Hessen mine (Dietrich 1978) as well as lacustrine argillaceous sandstones intercalated with Jurassic brown coal seams in the Kostanay region of Kazakhstan (Vertushkov 1952). Previous work mainly dealt with the crystallographic classification (e.g., Taborszki 1977; Dietrich 1978; Goth 1990; Fleck and Kolitsch 2003).

In the marker horizon M, messelite in the upper and lower band encloses single black pelite layers and packages of up to five laminae (Fig. 2). All platelets show the same degree of compaction, regardless of their spatial position. The intercalated black pelite shows that portions of the marker horizon precursor material had a composition like the bulk black pelite of the Messel pit. Evidently, the sedimentation of black pelite, algae layers, and marker horizon precursor material lasted several years. The subsequent diagenetic messelite formation resulted from the reaction of migrating phosphorus from organic material layers and mineral surfaces, and elements crucial for messelite precipitation, e.g., Fe and Ca, from the tephra (Table 1). Small ash particles with a large specific surface area and high dissolution rate are especially susceptible to early diagenetic dissolution (Wilson 2004). These reactive minerals comprise, e.g., olivine, pyroxene, and amphibole. Dissolution of these minerals readily liberates Fe and Ca for messelite formation into solution. The low Al concentration of messelite suggests that plagioclase dissolution played only a minor role in Ca liberation, while the presence of ferrous Fe (Table 1) indicates reducing conditions likely associated with hydrocarbon mobilization. Continuous messelite crystal growth in the lower and upper band fractured and disturbed the black pelite layers within the marker horizon. This indicates that the formation of the black pelite was completed when messelite crystal growth began and that,

contrary to previous interpretations (Schaal et al. 1987; Goth 1990; Felder 2007; Tütken 2014), the marker horizon M did not precipitate directly at the sediment–water interface but formed diagenetically.

Central montgomeryite globule band

Sharp mineralogical and textural boundaries between the messelite bands and the central messelite–montgomeryite–mantienneite band indicate an abrupt change of the marker horizon precursor composition. The central band is characterized by a specific order of phosphate precipitation, as well as trace mineral type and abundance, and the absence of black pelite relicts. The textural relationships suggest the following precipitation sequence (Fig. 5): (1) a messelite groundmass, (2) montgomeryite globules, (3) mantienneite, and (4) late vertical messelite veins with similar composition to the earlier bands.

The precursor to messelite in the central band is completely altered, with only a few silica spheres left. The dissolution of messelite and replacement by montgomeryite (Fig. 3b) releases Fe to the pore fluid that may migrate and form iron oxide/hydroxide elsewhere. Phosphorus from the alteration of messelite and organic matter is incorporated into montgomeryite. At low pH, the alteration of detrital apatite (Fig. 3c) can also provide P for montgomeryite formation (Nriagu 1976). Compared to messelite, montgomeryite contains large amounts of aluminum, ~ 0.1 vs ~ 16 wt% Al_2O_3, respectively (Table 1). Since messelite dissolution provides only negligible amounts of aluminum, dissolving feldspar and other Al-rich minerals are required as a local source for an Al-rich microenvironment. While aluminum is considered fluid immobile at circumneutral pH in low-temperature settings, its mobility increases significantly at low pH (10^{-3} mol/kg at pH 3; Curtis 1983). Migrating hydrocarbons from remnant dissolving organic compounds in- and outside the marker horizon are a likely source of this acidic (probably reducing) pore fluid. Subsequent montgomeryite precipitation may induce a concentration gradient that promotes Al diffusion toward mineral surfaces and facilitates montgomeryite globule formation (Fig. 3a).

Mantienneite authigenesis

The authigenesis of mantienneite documents an exceptional sedimentation episode during the formation of the Messel black pelite and the marker horizon M. To date, mantienneite has been analytically identified at three locations worldwide (including this study)—Anloua (Cameroon), Pinciná (Slovakia), and Messel (Germany). All three locations share a common association of lithologies dominated by clay minerals and organic matter. Mantienneite was first described by Fransolet et al. (1984) from

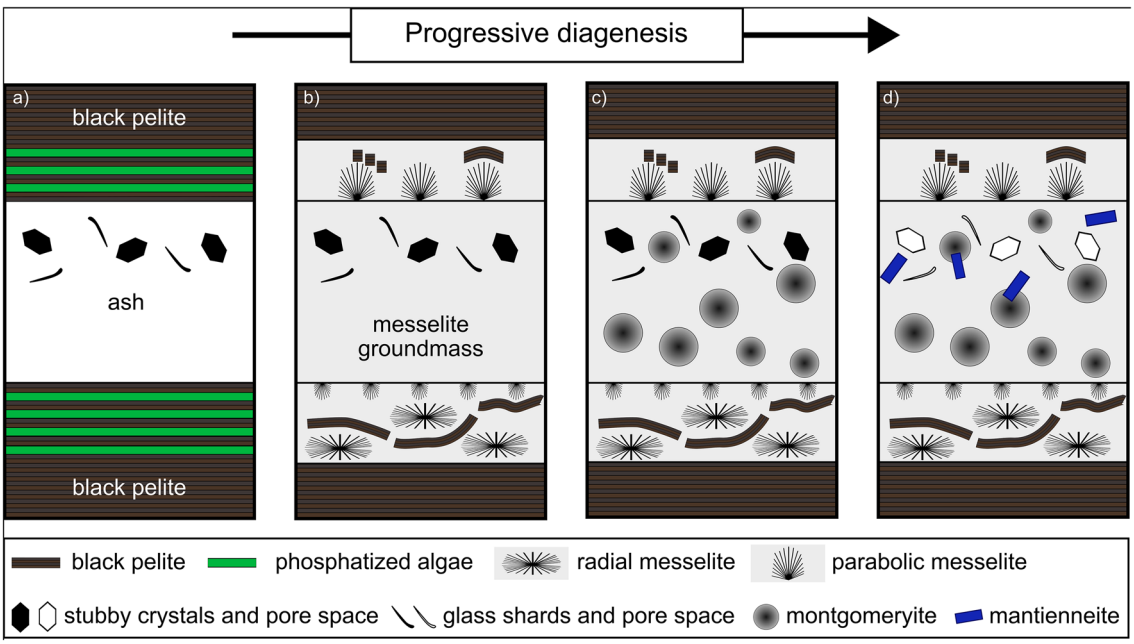

Fig. 5 Schematic representation of the crystallization sequence of the marker horizon during progressive diagenesis, **a** A layer of tephra surrounded with black pelite precursor material and algae layers preceded the phosphate mineral horizon, **b** Black pelite in the lower and upper band is bent and fractured by parabolic and radial messelite crystal growth, **c** Montgomeryite globules form in the messelite groundmass of the central band, followed by localized mantienneite precipitation (**d**) due to dissolution of stubby prismatic crystals, glass shards, messelite, and montgomeryite

the vivianite deposit of Anloua (Cameroon), a series of lacustrine deposits of Upper Tertiary to Quaternary age. In this series spherulites of mantienneite, a clay fraction, and siderite cement a black bituminous argillite with some thin sandy layers. A second occurrence is an alginate deposit near Pinciná, Slovakia (Vavrová et al. 2006). The alginate, a mixture of organic matter and clay minerals, was deposited in the Pinciná Maar lake that formed during Upper Miocene–Pliocene basalt volcanic activity (Hurai et al. 2021). Well-developed mantienneite spheres composed of radiating crystals occur in trace amounts in some horizons dominated by smectite and kaolinite. A hydrothermal overprint of microbially degraded algae and basaltic volcaniclastics at the maar surface has been suspected to induce mantienneite precipitation directly from solution (Vavrová et al. 2006). However, a hydrothermal overprint of the Middle Messel Formation black pelite has not been reported yet. We infer that the textural dissolution–precipitation relationships between the phosphate minerals in the central band show that mantienneite did not crystallize directly from a solution at the lake-sediment surface.

The dissolution of messelite and montgomeryite can provide Al and P required for mantienneite precipitation (Table 1). Mantienneite authigenesis also requires a local increase of the Mg, K, and Ti activity. The dissolution of minerals, such as pyroxene, alkali feldspar, biotite, and amphibole likely provided Mg and K. BSE images show that mantienneite replaces all other phosphates, which means that local dissolution of detrital Ti-rich minerals, e.g., Ti-augite, Ti-rich amphibole, biotite, and ilmenite must have liberated additional Ti. This agrees well with previous studies that interpreted mantienneite authigenesis in sediments rich in clay minerals and organic matter to result from the reaction of phosphorus-rich solutions with altering minerals, e.g., titanian augite and ilmenite (Fransolet et al. 1984). The silica sphere-filled pore space resembling stubby euhedral crystals in mantienneite (Fig. 4d) could be remnants after dissolution of such detrital minerals. Similarly to aluminum, Ti is usually fluid immobile in low-temperature geological systems, but its mobility increases considerably in low pH fluids rich in dissolved organic compounds (Hausrath et al. 2009; Fuchs et al. 2015; Schulz et al. 2016; Liu et al. 2019; Sindern et al. 2019). Kerogen maturation likely generates an acidic, reducing fluid, which also intensifies the leaching of detrital minerals, e.g., ilmenite (Weibel and Friis 2004). However, an increased titanium mobility at low pH, at least on the microscale, is commonly associated with oxidizing conditions (Weibel 1998; Sindern et al. 2019). Further, the presence of ferric Fe in mantienneite and precipitation of iron oxide/hydroxide indicates oxidizing conditions during mantienneite formation. The mantienneite-forming reaction, thus, marks the change from a regime of reducing to oxidizing conditions, possibly upon exhaustion of the dissolved organic compounds. Vertical messelite veins cross-cutting the entire marker horizon demonstrate that later kerogen maturation created another pulse of reducing pore fluid from below the marker horizon.

Conclusions

Our X-ray powder diffraction and electron beam microanalysis of the marker Horizon M of the Middle Eocene Middle Messel Formation provide strong evidence for a so far unidentified and exceptional tephra layer. Both, the solitary ash layer and a large supply of phosphorus from altering bacteria and algae layers were mandatory for the formation of the marker horizon. The tripartite marker horizon of phosphate minerals consists of bands of messelite crystal aggregates intercalated with black pelite enclosing a central montgomeryite-rich band. Fragmented and deformed black pelite laminae in the messelite bands directly evidence that the marker horizon formed diagenetically and not, as previously suggested (Schaal et al. 1987; Goth 1990; Felder 2007), at the sediment–lake interface. Mantienneite is identified for the first time in this deposit and only the third documented sedimentary occurrence worldwide.

Events such as turbidites from the crater wall or the shoreline cannot be considered as a source for the marker horizon precursor, since they occur frequently in the black pelite succession, but do not exhibit similar phosphatization phenomena. Most likely, an exogenous, wind-driven event, specifically a volcanogenic ash, provided most of the material forming the marker horizon.

The textural and chemical relationships in the marker horizon suggest a diagenetic precipitation sequence of messelite, montgomeryite globules, and mantienneite that formed in the presence of dissolving Ti-rich minerals, such as ilmenite and Ti-rich pyroxene. A marked Al and Ti mobility is likely linked to kerogen maturation that produced acidic, reducing pore fluids with high P concentration. The singular depositional conditions and the resulting phosphorus diffusion from altering volcanogenic ash and algae layers during diagenesis were exceptional in a timespan of about 640 kyr of stable facies conditions and sedimentation rate.

Acknowledgements We sincerely thank the Editor-in-Chief Ulrich Riller, Topic Editor Nora Noffke, Olaf K. Lenz, and an anonymous reviewer for their detailed and thoughtful comments. Both authors thank Timm John (Freie Universität Berlin) for access to X-ray diffraction and electron microbeam facilities. Michael Wuttke thanks Marita Felder for preliminary work and Dieter Uhl for providing a workplace in the Section for Palaeoclimate and Environmental Research (Senckenberg, Frankfurt M). The authors acknowledge discussions with Louis Jung (Berlin), Georg Büchel (Jena), Peter Suhr (Dresden), and Jan Pleuger (Berlin), and support by the Open Access Publication Fund of

the Freie Universität Berlin. Open Access funding enabled and organized by Projekt DEAL.

Author contributions All authors contributed to the study conception and design. Material preparation was performed by Michael Wuttke and Moritz Liesegang. Data collection and analysis were performed by Moritz Liesegang. The first draft of the manuscript was written together by both authors that also commented on previous versions of the manuscript. All authors read and approved the final manuscript.

Funding No specific funding was provided for the analyses of this study. Open Access funding enabled and organized by Projekt DEAL.

Availability of data and materials All datasets for this research are included in this study. In addition, primary XRD data are available in the Zenodo Repository, at https://doi.org/10.5281/zenodo.6406833.

Code availability Not applicable.

Declarations

Conflict of interest The authors declare that they have no known competing financial interests or personal relationships that could have appeared to influence the work reported in this paper.

Consent for publication All authors agreed with the content and gave explicit consent to submit the manuscript.

References

Bauersachs T, Schouten S, Schwark L (2014) Characterization of the sedimentary organic matter preserved in Messel oil shale by bulk geochemistry and stable isotopes. Palaeogeogr Palaeoclimat Palaeoecol 410:390–400. https://doi.org/10.1016/j.palaeo.2014.06.015

Berger J-P, Reichenbacher B, Becker D, Grimm M, Grimm K, Picot L, Storni A, Pirkenseer C, Schaefer A (2005a) Eocene-Pliocene time scale and stratigraphy of the Upper Rhine Graben (URG) and the Swiss Molasse Basin (SMB). Int J Earth Sci (geol Rundsch) 94:711–731. https://doi.org/10.1007/s00531-005-0479-y

Berger J-P, Reichenbacher B, Becker D, Grimm M, Grimm K, Picot L, Storni A, Pirkenseer C, Derer C, Schaefer A (2005b) Paleogeography of the Upper Rhine Graben (URG) and the Swiss Molasse Basin (SMB) from Eocene to Pliocene. Int J Earth Sci 94:697–710. https://doi.org/10.1007/s00531-005-0475-2

Browning TJ, Stone K, Bouman HA, Mather TA, Pyle DM, Moore CM, Martinez-Vicente V (2015) Volcanic ash supply to the surface ocean—remote sensing of biological responses and their wider biogeochemical significance. Front Mar Sci 2:14. https://doi.org/10.3389/fmars.2015.00014

Büchel G, Schaal SFK (2018) Chapter 2. The formation of the Messel Maar. In: Smith KT, Schaal SFK, Habersetzer J (Eds) Messel. An ancient Greenhouse Ecosystem. Senckenberg, Frankfurt M, pp 7–16

Chen M, Ding S, Chen X, Sun Q, Fan X, Lin J, Ren M, Yang L, Zhang C (2018) Mechanisms driving phosphorus release during algal blooms based on hourly changes in iron and phosphorus concentrations in sediments. Water Res 133:153–164. https://doi.org/10.1016/j.watres.2018.01.040

Cosmidis J, Benzerara K, Morin G, Busigny V, Lebeau O, Jézéquel D, Noël V, Othmane Dublet G, (2014) Biomineralization of iron-phosphates in the water column of Lake Pavin (Massif Central, France). Geochim Cosmochim Acta 126:78–96. https://doi.org/10.1016/j.gca.2013.10.037

Curtis CD (1983) Link between aluminum mobility and destruction of secondary porosity. AAPG Bull 67:380–384. https://doi.org/10.1306/03B5AD22-16D1-11D7-8645000102C1865D

Dietrich R (1978) Das Messelitproblem: Messelit und Anapaite aus dem Ölschiefer von Messel. Aufschluß 29:229–233

Duggen S, Croot P, Schacht U, Hoffmann L (2007) Subduction zone volcanic ash can fertilizethe surface ocean and stimulate phytoplankton growth: Evidence from biogeochemical experiments and satellite data. Geophys Res Lett 34:L01612. https://doi.org/10.1029/2006GL027522

Felder M, Harms F-J (2004) Lithologie und genetische Interpretation der vulkano-sedimentären Ablagerungen aus der Grube Messel anhand der Forschungsbohrung Messel 2001 und weiterer Bohrungen. Cour for Senckenbg 252:151–203

Felder M (2001) Paläolimnologische Untersuchungen zu Siderit- und Aragonitbildung in schwarzpelitdominierten, paläogenen Seen Mitteleuropas. Dissertation, Friedrich-Schiller-Universität Jena

Felder M (2007) Phosphatminerale im Messeler Ölschiefer.. In: Jäger P, Königshof P, Veit-Köhler G, Wenzel T (eds) Senckenberg 2005–2006. Senckenbg Naturf Ges, Frankfurt M, pp 38–39

Fleck M, Kolitsch U (2003) Natural and synthetic compounds with kröhnkite-type chains. An Update Z Kristallogr 218:553–567. https://doi.org/10.1524/zkri.218.8.553.20689

Fransolet A-M, Oustrière P, Fontan F, Pillard F (1984) La mantienéite, une nouvelle espèce minérale du gisement de vivianite d'Anloua, Cameroun. Bull Minéral 107:737–744. https://doi.org/10.3406/bulmi.1984.7815

Franzen JL, Weber J, Wuttke M (1982) Senckenberg-Grabungen in der Grube Messel bei Darmstadt. 3. Ergebnisse 1979–1981. Cour for Senckenbg 54:1–118

Fuchs S, Schumann D, Williams-Jones AE, Vali H (2015) The growth and concentration of uranium and titanium minerals in hydrocarbons of the Carbon Leader Reef, Witwatersrand Supergroup, South Africa. Chem Geol 393:55–66. https://doi.org/10.1016/j.chemgeo.2014.11.018

Gao Y, Cornwell JC, Stoecker DK, Owens MS (2014) Influence of cyanobacteria blooms on sediment biogeochemistry and nutrient fluxes. Limnol Oceanogr 59:959–971. https://doi.org/10.4319/lo.2014.59.3.0959

Goth K (1990) Der Messeler Ölschiefer – ein Algenlaminit. Cour for Senckenbg 131:1–143

Hamilton DS et al (2022) Earth, wind, fire, and pollution: Aerosol nutrient sources and impacts on ocean biogeochemistry. Ann Rev Mar Sci 14:303–330. https://doi.org/10.1146/annurev-marine-031921-013612

Hamme RC et al (2010) Volcanic ash fuels anomalous plankton bloom in subarctic northeast Pacific. Geophys Res Lett 37:L19604. https://doi.org/10.1029/2010GL044629

Harms FJ, Wallner H, Jacoby WR (1999) Karte zur Verbreitung der Messel-Formation/Faltblatt Welterbe Grube Messel—Map, back side with comment. Hess L-Amt Bodenforsch

Hausrath EM, Neaman A, Brantley SL (2009) Elemental release rates from dissolving basalt and granite with and without organic ligands. Am J Sci 309:633–660. https://doi.org/10.2475/08.2009.01

Huber H, Koeberl C, Egger H (2003) Geochemical study of lower Eocene volcanic ash layers from the Alpine Anthering Formation, Austria. Geochem J 37:123–134. https://doi.org/10.2343/geochemj.37.123

Hurai V, Huraiová M, Konečný P (2021) REE minerals as geochemical proxies of Late-Tertiary alkalic silicate ± carbonatite intrusions beneath Carpathian Back-Arc Basin. Minerals 11:369. https://doi.org/10.3390/min11040369

Jacoby W, Wallner H, Smilde P (2000) Tektonik und Vulkanismus entlang der Messeler Störungszone auf dem Sprendlinger Horst: Geophysikalische Ergebnisse. Z Dtsch Geol Ges 151:493–510. https://doi.org/10.1127/zdgg/151/2001/493

Kubanek F, Nöltner T, Weber J, Zimmerle W (1988) On the lithogenesis of the Messel oilshale. Cour for Senckenbg 107:13–28

Lenz OK, Wilde V (2018) Changes in Eocene plant diversity and composition of vegetation: The lacustrine archive of Messel (Germany). Palaeobiol 44:1–27. https://doi.org/10.1017/pab.2018.25

Lenz OK, Wilde V, Riegel W, Heinrichs T (2007) Distribution and paleoecologic significance of the freshwater dinoflagellate cyst *Messelodinium thielepfeifferae* gen. et sp. nov from the Middle Eocene of Lake Messel. Germany Palynol 31:119–134. https://doi.org/10.1080/01916122.2007.9989639

Lenz OK, Wilde V, Riegel W (2011) Short-term fluctuations in vegetation and phytoplankton during the Middle Eocene greenhouse climate: a 640-kyr record from the Messel oil shale (Germany). Int J Earth Sci 100:1851–1874. https://doi.org/10.1007/s00531-010-0609-z

Lenz OK, Wilde V, Mertz DF, Riegel W (2015) New palynology-based astronomical and revised $^{40}Ar/^{39}Ar$ ages for the Eocene maar lake of Messel (Germany). Int J Earth Sci 104:873–889. https://doi.org/10.1007/s00531-014-1126-2

Liebig K, Westall F, Schmitz M (1996) A study of fossil microstructures from the Eocene Messel Formation using transmission electron microscopy. N Jb Geol Paläont Mh 1996:218–231. https://doi.org/10.1127/njgpm/1996/1996/218

Liesegang M, Milke R (2014) Australian sedimentary opal-A and its associated minerals: Implications for natural silica sphere formation. Am Mineral 99:1488–1499. https://doi.org/10.2138/am.2014.4791

Liu ZRR, Zhou MF, Williams-Jones AE, Wang W, Gao JF (2019) Diagenetic mobilization of Ti and formation of brookite/anatase in early Cambrian black shales, South China. Chem Geol 506:79–96. https://doi.org/10.1016/j.chemgeo.2018.12.022

Lu J, Zhang P, Dal Corso J, Yang M, Wignall PB, Greene SE, Shao L, Lyu D, Hilton J (2021) Volcanically driven lacustrine ecosystem changes during the Carnian Pluvial Episode (Late Triassic). Proc Natl Acad Sci USA 118:e2109895118. https://doi.org/10.1073/pnas.2109895118

Lutz H, Lorenz V, Engel T, Häfner F, Haneke J (2013) Paleogene phreatomagmatic volcanism on the western main fault of the northern Upper Rhine Graben (Kisselwörth diatreme and Nierstein-Astheim Volcanic System, Germany). Bull Volcanol 75:741. https://doi.org/10.1007/s00445-013-0741-2

Maccaferri F, Rivalta E, Keir D, Acocella V (2014) Off-rift volcanism in rift zones determined by crustal unloading. Nature Geosci 7:297–300. https://doi.org/10.1038/ngeo2110

Marell D (1989) Das Rotliegende zwischen Odenwald und Taunus. Geol Abh Hessen 89:1–128

Matthess G (1966) Zur Geologie des Ölschiefervorkommens von Messel bei Darmstadt. Abh Hess L-Amt Bodenforsch 51:1–87

Matthews-Bird F, Brooks SJ, Gosling WD, Gulliver P, Mothes P, Montoya E (2017) Aquatic community response to volcanic eruptions on the Ecuadorian Andean flank: evidence from the palaeoecological record. J Paleolimnol 58:437–453. https://doi.org/10.1007/s10933-017-0001-0

Mertz DF, Renne PR (2005) A numerical age for the Messel fossil deposit (UNESCO World Heritage) derived from $^{40}Ar/^{39}Ar$ dating on a basaltic rock fragment. Cour for Senckenbg 255:67–75

Meyer R, van Wijk J, Gernigon L (2007) The North Atlantic Igneous Province: A review of models for its formation. Geol Soc Am Spec Pap 430:525–552. https://doi.org/10.1130/2007.2430(26)

Mezger JE, Felder F, Harms F-J (2013) Crystalline rocks in the maar deposits of Messel: key to understand the geometries of the Messel Fault Zone and diatreme and the post-eruptional development of the basin fill. Z Dtsch Ges Geowiss 164:639–662. https://doi.org/10.1127/1860-1804/2013/0034

Michon L, Merle O (2001) The evolution of the Massif Central Rift; spatio-temporal distribution of the volcanism. Bull Soc Géol Fr 172:201–211. https://doi.org/10.2113/172.2.201

Micklich N (2002) The fish fauna of Messel Pit: a nursery school? Cour for Senckenbg 237:97–127

Micklich N (2012) Peculiarities of the Messel fish fauna and their palaeoecological implications: a case study. Palaeobiodiv Palaeoenv 92:585–629. https://doi.org/10.1007/s12549-012-0106-4

Modenutti BE, Balseiro EG, Elser JJ, Navarro MB, Cuassolo F, Laspoumaderes C, Souza MS, Villanueva VD (2013) Effect of volcanic eruption on nutrients, light, and phytoplankton in oligotrophic lakes. Limnol Oceanogr 58:1165–1175. https://doi.org/10.4319/lo.2013.58.4.1165

Moshayedi M, Lenz OK, Wilde V (2018) Controls on sedimentation and vegetation in an Eocene pull-apart basin (Prinz von Hessen, Germany): Evidence from palynology. J Geol Soc 175:757–773. https://doi.org/10.1144/jgs2017-128

Moshayedi M, Lenz OK, Wilde V, Hinderer M (2020) The recolonisation of volcanically disturbed Eocene habitats of Central Europe: the maar lakes of Messel and Offenthal (SW Germany) compared. Palaeobiodiv Palaeoenv 100:951–973. https://doi.org/10.1007/s12549-020-00425-4

Muthmann W (1890) Messelit, ein neues Mineral. Z Krystallogr Min 17:93–94

Nitzsche T, Rolf C, de Wall H (2006) Origin of magnetic anomalies in volcaniclastic units of the Messel maar-diatreme (Germany). Z Dtsch Ges Geowiss 157:373–385. https://doi.org/10.1127/1860-1804/2006/0157-0373

Nriagu JO (1976) Phosphate-clay mineral relations in soils and sediments. Canadian J Earth Sci 13:717–736. https://doi.org/10.1139/e76-077

Pe-Piper G, Karim A, Piper DJ (2011) Authigenesis of titania minerals and the mobility of Ti: new evidence from pro-deltaic sandstones, Cretaceous Scotian Basin, Canada. J Sed Res 81:762–773. https://doi.org/10.2110/jsr.2011.63

Porder S, Ramachandran S (2013) The phosphorus concentration of common rocks - a potential driver of ecosystem P status. Plant Soil 367:41–55. https://doi.org/10.1007/s11104-012-1490-2

Reischmann, T. (2011). Tertiärer Vulkanismus. – In: Grimm, K.I. (coord.), Stratigraphie von Deutschland IX, Tertiär, Teil 1: Oberrheingraben und benachbarte Gebiete. Schr.reihe Dtsch Ges Geowiss 75:16–30.

Richter G, Schiller W, Baszio S (2013) A green alga of the genus *Coelastrum* Naegeli from the sediments of the Tertiary Lake Messel. Palaeobiodiv Palaeoenv 93:285–298. https://doi.org/10.1007/s12549-012-0105-5

Richter G, Baszio S, Wuttke M (2017) Discontinuities in the microfossil record of middle Eocene Lake Messel: clues for ecological changes in lake's history? Palaeobiodiv Palaeoenv 97:295–314. https://doi.org/10.1007/s12549-016-0254-z

Ruiz-Agudo E, Putnis CV, Putnis A (2014) Coupled dissolution and precipitation at mineral–fluid interfaces. Chem Geol 383:132–146. https://doi.org/10.1016/j.chemgeo.2014.06.007

Schaal S, Schmitz-Münker M, Wolf H-G (1987) Neue Korrelationsmöglichkeiten von Grabungsstellen in der eozänen Fossillagerstätte Grube Messel. Cour for Senckenbg 91:203–210

Schaal S (1992) The genesis of the Messel oil shale. In: Schaal S, Ziegler W (Eds) Messel. An insight into the history of life and of the earth. Clarendon Press, Oxford.

Schmitz M (1991) Die Koprolithen mitteleozäner Vertebraten aus der Grube Messel bei Darmstadt. Cour for Senckenbg 137:1–159

Schulz R, Harms F-J, Felder M (2002) Die Forschungsbohrung Messel 2001: Ein Beitrag zur Entschlüsselung der Genese einer Ölschieferlagerstätte. Z Angew Geol 2002:9–17

Schulz HM, Wirth R, Schreiber A (2016) Nano-crystal formation of TiO_2 polymorphs brookite and anatase due to organic–inorganic rock-fluid interactions. J Sed Res 86:59–72. https://doi.org/10.2110/jsr.2016.1

Sindern S, Havenith V, Gerdes A, Meyer FM, Adelmann D, Hellmann A (2019) Dating of anatase-forming diagenetic reactions in Rotliegend sandstones of the North German Basin. Int J Earth Sci 108:1275–1292. https://doi.org/10.1007/s00531-019-01705-x

Sissingh W (2003) Tertiary paleogeographic and tectonostratigraphic evolution of the Rhenish Triple Junction. Palaeogeog Palaeoclimat Palaeoecol 196:229–263. https://doi.org/10.1016/S0031-0182(03)00320-1

Smith L, Watzin MC, Druschel G (2011) Relating sediment phosphorus mobility to seasonal and diel redox fluctuations at the sediment–water interface in a eutrophic freshwater lake. Limnol Oceanogr 56:2251–2264. https://doi.org/10.4319/lo.2011.56.6.2251

Taborszki K (1977) Der Messelit und das Messelitproblem. Ber Naturf Ges Freiburg 67:335–345

Tütken T (2014) Isotope compositions (C, O, Sr, Nd) of vertebrate fossils from the Middle Eocene oil shale of Messel, Germany: implications for their taphonomy and palaeoenvironment. Palaeogeog Palaeoclimat Palaeoecol 416:92–109. https://doi.org/10.1016/j.palaeo.2014.08.005

Vavrová J, Biron A, Galko I (2006) Mantienneite – A new phosphate mineral from alginite deposit (Pinciná, Slovakia). Mineral Polonica – Spec Pap 28: 232–234

Vertushkov GN (1952) Messelite from the Kostanay region. Zapiski Vsesojuzn Mineralogy Obsccesva 81:207–208 ((**in Russian**))

Waldmann S, Gaupp R (2016) Grain-rimming kaolinite in Permian Rotliegend reservoir rocks. Sed Geol 335:17–33. https://doi.org/10.1016/j.sedgeo.2016.01.016

Wang J, Zhou Y, Bai X, Li W (2022) Effect of algal blooms outbreak and decline on phosphorus migration in Lake Taihu. China Environ Pollut 296:118761. https://doi.org/10.1016/j.envpol.2021.118761

Weber J, Hofmann U (1982) Kernbohrungen in der eozänen Fossillagerstätte Grube Messel bei Darmstadt. Geol Abh Hess 83:1–58

Weber J, Zimmerle W (1985) Pyroclastic detritus in the lacustrine sediments of the Messel Formation. Senck Laeth 66:171–176

Weber J (1988) Sedimentpetrographische Untersuchungen in der eozänen Messel-Formation. Dissertation, Johann Wolfgang Goethe-Universität Frankfurt am Main

Weibel R (1998) Diagenesis in oxidising and locally reducing conditions — an example from the Triassic Skagerrak Formation, Denmark. Sed Geol 121:259–276. https://doi.org/10.1016/S0037-0738(98)00085-2

Weibel R, Friis H (2004) Opaque minerals as keys for distinguishing oxidising and reducing diagenetic conditions in the Lower Triassic Bunter Sandstone, North German Basin. Sed Geol 169:129–149. https://doi.org/10.1016/j.sedgeo.2004.05.004

Wilkinson CM, Morgan G, Hendriksi BWH, Eide EA (2017) Compilation and appraisal of geochronological data from the North Atlantic Igneous Province (NAIP). In: Péron-Pinvidic G, Hopper, JR, Stoker MS, Gaina C, Doornenbal JC, Funck T, Árting UE (eds) The NE Atlantic Region: A Reappraisal of Crustal Structure, Tectonostratigraphy and Magmatic Evolution. Geol Soc London Spec Publ, pp 69–103. https://doi.org/10.1144/SP447.10

Wilson MJ (2004) Weathering of the primary rock-forming minerals: processes, products and rates. Clay Miner 39:233–266. https://doi.org/10.1180/0009855043930133